


Spatially Resolved Measurements of HNCO Hydrolysis over SCR Catalysts

Mario Eck¹, Patrick Lott¹, David Schweigert^{1,2}, Marion Börnhorst¹, and Olaf Deutschmann^{1,*}

DOI: 10.1002/cite.202100192

 This is an open access article under the terms of the Creative Commons Attribution-NonCommercial License, which permits use, distribution and reproduction in any medium, provided the original work is properly cited and is not used for commercial purposes.



Supporting Information
available online

In order to understand deposit formation during urea selective catalytic reduction (SCR) resulting from isocyanic acid (HNCO) formation, the present study investigates the potential of HNCO hydrolysis by spatially resolved gas phase concentration profiles along a single catalyst channel of commercial Cu-zeolite and V-based SCR catalysts. The spatially resolved profiles, obtained in a special hot gas test rig via capillary technique, provide information on reaction rates of HNCO hydrolysis, NH₃ adsorption and NO conversion, hereby revealing a better performance of the standard V-based catalyst regarding the HNCO hydrolysis, which is attributed to the TiO₂ support.

Keywords: HNCO hydrolysis, In situ sampling, Selective catalytic reduction, Spatial profiling

Received: October 29, 2021; *revised:* March 11, 2022; *accepted:* March 16, 2022

1 Introduction

On the way towards a sustainable and modern energy system, combustion engines will remain indispensable during the transition period until new technologies are established. In this respect, particularly modern lean-burn engines with their high efficiency still experience significant interest, e.g., in large-bore applications. Although engine-related measures and state-of-the-art exhaust gas aftertreatment systems ensure low levels of emissions, the ever-tightening emission limits that consecutively comprise more and more pollutants require continuous advances in aftertreatment technologies. Irrespective whether the engine is fueled by diesel, natural gas or hydrogen, the efficient reduction of nitrogen oxides (NO_x) is particularly challenging. Commonly, the selective catalytic reduction (SCR) represents the state-of-the-art deNO_x technology for reducing NO_x emissions in lean exhausts. [1–4]

While the opportunity of using hydrogen as a reductant is currently under evaluation for deNO_x of the exhaust of hydrogen-fueled combustion engines [5–7], the predominant system for NO_x removal uses ammonia (NH₃) as reducing agent, which is generated from a urea-water solution (UWS) that serves as liquid precursor for NH₃. Thermal decomposition of the injected urea spray results in formation of one equivalent NH₃ and the intermediate species isocyanic acid (HNCO) (Eq. (1)).



Ideally, the subsequent hydrolysis of HNCO results in further NH₃ formation (Eq. (2)). However, HNCO can oligomerize and polymerize to undesired solid urea derivatives such as biuret, triuret or cyanuric acid [8–11]. These solid residues decompose slowly even at higher temperatures, which potentially results in an inhomogeneous NH₃ distribution as well as a potential blockage of the catalyst and the upstream tailpipe [10]. Hence, deposition management represents a major challenge in the development of robust exhaust gas aftertreatment systems, especially since modern aftertreatment systems are reduced in size for a close-coupled position to the engine offering only a short mixing section. If the HNCO does not form deposits and is not further converted over the SCR catalyst, it can be emitted, which represents an equally important issue, since HNCO presumably causes cardiovascular and respiratory diseases [12]. All these issues need to be addressed for both current and future technologies.

However, the conversion of HNCO via hydrolysis is a slow process due to HNCO being highly stable in the gas

¹Mario Eck, Dr. Patrick Lott, Dr. David Schweigert, Dr. Marion Börnhorst, Prof. Dr. Olaf Deutschmann
deutschmann@kit.edu

Karlsruhe Institute of Technology, Institute for Chemical Technology and Polymer Chemistry, Engesserstraße 18, 76131 Karlsruhe, Germany.

²current address:

cellcentric GmbH & Co. KG, Neue Straße 95, 73230 Kirchheim/Teck-Nabern, Germany.

phase. Observations at around 250–400 °C and a residence time above 0.1 s [13, 14] show equivalent concentrations of NH₃ and HNCO after urea thermolysis, concluding that HNCO cannot be efficiently hydrolyzed by those relatively long mixing distances (high residence time) in this temperature range. Thus, an efficient approach to achieve a fast HNCO hydrolysis is either using a dedicated catalyst for the hydrolysis or modifying the SCR catalyst to promote the thermolysis of urea and subsequent HNCO hydrolysis (Eqs. (1), (2)). By using V₂O₅/WO₃-TiO₂ (VWT), Goldbach et al. demonstrated that SCR catalysts are already a suitable starting point to hydrolyze HNCO in urea SCR [15]. However, their main purpose is catalyzing the selective reduction reaction. Experimental investigations by Kröcher et al. [16] revealed a residual fraction of up to 80 ppm HNCO out of 800 ppm N-reductant (NH₃ in this case) in the exhaust gas during operation at 230 °C and a deNO_x value of 63 %, using a VWT catalyst. Tests at these low temperatures clearly demonstrated an HNCO slip especially when using aged catalysts. Similarly, studies under worldwide harmonized light duty test cycle (WLTC) conditions [17] detected HNCO downstream the catalyst during low temperature operation (< 250 °C). Hence, efficient and complete HNCO hydrolysis should be ensured for an efficient exhaust gas aftertreatment system, particularly for urban traffic where low temperatures occur comparably often.

Catalyst formulations commonly applied for selective catalytic reduction at low temperatures are Cu-zeolites and VWT catalysts [13–15, 18–24]. Both types have been subject to numerous scientific studies in the past and are meanwhile well-established in industry. While NO and NH₃ typically adsorb on Cu or V sites, the support material further contributes to the catalytic activity. Both, zeolitic and VWT catalysts are able to store NH₃ to a certain extent, which are released at higher temperatures and lower gas-phase concentration of NH₃, supporting the deNO_x process. [21]

However, the optimal operating conditions for complete HNCO conversion are still subject of debate, with special recommendations for the different catalytic materials, e.g., an operating temperature above 200 °C for VWT catalysts [14, 15]. Especially at low temperature, a vanadia-based catalyst is favored due to its pronounced fast SCR activity and at the same time provision of specific active sites on TiO₂ for HNCO hydrolysis [22]. VWT catalysts might be favored for HNCO hydrolysis, since not only the active species V₂O₅ offers adsorption sites, but also the support material itself. In fact, HNCO rather adsorbs on the TiO₂ surface than on V₂O₅ [25], which leaves the V-sites available for the subsequent SCR reaction between NO and NH₃. In addition, the catalyst structure can have a significant impact on the SCR activity [26]. The porous structure of zeolitic catalysts, for instance, can favor the creation of nitrates on the surface, which are an interim step of the SCR. However, these pores can accumulate urea and HNCO, blocking the active sites for the SCR reaction [27].

Due to the fundamental differences in their structural, physical and chemical properties, a direct comparison between Cu-zeolite and vanadia-titania-based catalysts in the context of HNCO hydrolysis is of interest. In addition to investigating the impact of the catalyst formulation, gas phase phenomena such as interactions between NO₂ and HNCO are worth to be considered. The presence of gas phase NO₂, for instance, inhibits titania's ability to catalyze HNCO hydrolysis, due to the formation of stable ammonium nitrate, blocking the active sites [28]. Moreover, instead of HNCO hydrolysis, also a direct interaction of HNCO with NO₂ is possible, which results in formation of HONO intermediates [29] that play a major role in the complex SCR mechanism [30]. In this context, profound insights into the gas phase and surface reactions are desirable, since they are a prerequisite for designing efficient catalysts and aftertreatment systems.

In our present study, we investigate the complex urea chemistry that has already been subject to earlier studies of our group [31–33] and particularly focus on HNCO formation and decomposition under realistic lean exhaust conditions by utilizing a hot gas test bench that comprises an UWS dosage upstream of an SCR catalyst. Incorporating axially movable capillaries connected to a mass spectrometer allows the measurement of spatially resolved concentration profiles along a single monolith channel. As demonstrated in previous research, spatial profiling is a powerful tool for understanding the changes of concentration and temperature along the monolithic catalyst and can contribute to unraveling multistep reactions in a wide variety of homo- and heterogeneous catalytic processes [34–41]. Such aspects are crucial for a fundamental understanding of the whole SCR process and HNCO abatement in particular. The concentration profiles of HNCO and other relevant gas species within commercial catalysts as presented herein are supplemented by a series of powder catalyst experiments that were conducted to investigate the hydrolysis of HNCO over TiO₂ and Cu-zeolites without urea dosage under model-like conditions. The experiments help to understand the interaction of UWS by-products with the catalyst surface, the related gas phase reactions within the monolith as well as the formation of deposits.

2 Experimental Section

This section describes the two experimental setups used for the experiments.

2.1 Powder Setup

The powder catalyst experiments under model conditions were conducted in an in-house built setup (Fig. S1 in the Supporting Information SI) dedicated to powder catalyst testing. A LabView software tool controls the entire setup

and simultaneously protocols all relevant data such as temperature, gas flow and gas species concentrations. The reaction gases are regulated by mass flow controllers (MFC, Bronkhorst) and stainless-steel pipes, which are preheated to 170 °C and which feed the reaction gas mixture into a quartz glass reactor that is located in a furnace (Gero). While the gases used are obtained from AirLiquid cylinders with a purity of 99.999 % for N₂, O₂ and H₂, water was formed by a reaction between hydrogen and oxygen over a platinum-based oxidation catalyst in order to create a steam-containing atmosphere. The total gas flow was set to 500 mL min⁻¹, which results in a gas hourly space velocity *GHSV* of 17 000 h⁻¹ within the catalyst bed. The catalyst bed consists of pure TiO₂ or Cu-ZSM-5 powder, respectively. For the tests with TiO₂, titanium(IV)oxide 1/8'' pellets (Alfa Aesar) were finely grinded, whereas Cu-ZSM-5 was prepared via incipient wetness impregnation by solving copper(II) acetate (≥ 99 %, Merck) in ultrapure water (Merck), subsequent drop-wise addition of the solution onto commercial ZSM-5 powder (ammonium-form, Alfa Aesar) and final drying at 75 °C. Both powders were calcined at 550 °C for 5 h before use. Thereafter, 100 mg of the catalyst powder (either TiO₂ or Cu-ZSM5) were fixed with quartz wool in a tubular quartz glass reactor with an inner diameter of 21 mm and approx. 15 mg of cyanuric acid (98 %, Sigma-Aldrich) were placed in a ceramic crucible that was positioned in front of the catalyst. After putting the reactor in a furnace, two thermocouples were placed directly over the cyanuric acid sample and behind the catalyst bed. The thermocouple above the cyanuric acid is used to operate the temperature ramp of the furnace via Eurotherm controllers. The end-of-pipe gas species concentrations were monitored by a Fourier-transform infrared (FTIR) spectrometer (MultiGas 2030, MKS). The measurement starts at 100 °C and finishes at 500 °C, while heating with a rate of 2 K min⁻¹.

2.2 Hot Gas Test Rig

Spatially resolved gas phase species concentrations within a single monolith channel of a catalyst substrate were obtained by implementing a capillary-based measurement extension into a hot gas test rig (Fig. S2), which was already described in detail in previous studies on UWS film and deposit formation [42]. This test rig can be operated under a wide range of parameters (temperature, flow velocity, mass flow of injected USW). For the present study, an operating point of 300 °C is chosen (Fig. S3), since especially low temperatures are challenging concerning HNCO hydrolysis. A radial compressor is supplying the atmosphere, blowing ambient air into the setup. The air (average velocity of 9.5 m s⁻¹) is heated with an inline electrical gas heater (Leister LE 5000 DF). Additionally, H₂O, NO and NH₃ can be dosed at the inlet section of the flow arrangement to ensure appropriate distribution. The flow enters a flow

straightener with a honeycomb structure and turbulence screens to homogenize flow and reduce turbulence. The injection section (length of 200 mm) is optically accessible through borosilicate windows. For UWS dosage, a commercial three-hole injector (Bosch Denoxtronic) is mounted with an inclination angle of 33° on the measurement section. This ensures a suitable spray distribution in front of the catalyst. UWS (AdBlue, EuroLub) is injected with a mass flow of 0.5 g min⁻¹ and an injection pressure of 5 bar. The urea decomposes into NH₃ and HNCO and the resulting concentration is measured end-of-pipe via FTIR (MultiGas 2030, MKS). At the applied temperature of 300 °C, an equimolar yield of NH₃ and HNCO is assumed based on literature data reporting low hydrolysis activity of HNCO in the gas phase [43]. In the catalyst chamber, either a commercially available Cu-zeolite or vanadia-titania-based catalyst system (150 mm long) is used.

The arrangement used to measure axial profiles of temperature and gas composition in the monolith inside the hot gas test rig is analogous to those already described in literature [34, 44]. To determine the concentration profiles, a deactivated, fused silica capillary with an outer diameter of 170 μm (I.D. = 100 μm) was used to reduce disturbances of the capillary on the gas flow to a minimum [45]. A low gas volume flow (approx. 1 mL min⁻¹ at standard conditions) is sucked through the capillary within the channel and guided into the mass spectrometer (HPR-20, Hiden Analytical), where the gas composition is analyzed. The FTIR measurements at the end of the pipe were used for calibration of the MS data, while an HNCO/NH₃ ratio of one was assumed upstream the catalyst. The sampling system is capable of simultaneously detecting a wide spectrum of gaseous species and mass balances are usually estimated within ±10 % error. Via a motorized linear stage (OptoSigma) the capillary is moved axially along the monolith channels (substrate coated with Cu-zeolite: 400 cps, 15 cm length; substrate coated with a vanadia-titania-based catalyst: 600 cps, 15 cm length), where data points are collected for 5 min at each sampling position. Each data point represents the averaged value over the last 3 min of measurement.

3 Results and Discussion

The results are presented in two sections, one focusing on the results from the powder setup for preliminary testing Cu-zeolite and TiO₂ for HNCO hydrolysis. Subsequently, experimental results of HNCO hydrolysis over Cu-zeolite and vanadia-titania-based catalysts under real conditions are discussed.

3.1 HNCO Hydrolysis over Different Catalysts

For the experiments at the powder setup, cyanuric acid, a side product of urea decomposition, is used as a HNCO precursor. Cyanuric acid sublimates during heat up and then decomposes to HNCO on the catalyst surface, before the formed HNCO hydrolyzes into NH_3 and CO_2 . Full conversion into those products serves as indicator for high catalytic activity. In order to ensure complete hydrolysis, 5 vol % water is added to the gas flow. Fig. 1 shows the concentration of HNCO, which is detected via an FTIR at the reactor outlet. The fact that no HNCO could be detected for the measurements with TiO_2 suggests a high catalytic activity of TiO_2 for HNCO decomposition, since full conversion into the hydrolysis products NH_3 and CO_2 is achieved (Fig. 1a).

Although the Cu-zeolite converts the isocyanic acid into its hydrolysis products, HNCO is still detected downstream the catalyst bed. The resulting molar quantities are calculated and converted into mass to compare them with the starting quantity. The results in Tab.1 reveal that the HNCO amount at the reactor outlet after passing the Cu-ZSM-5 catalyst equals to 1.2 mol% of the starting amount of HNCO from complete cyanuric acid decomposition.

Based on these results it shows TiO_2 is found to be more favorable as a urea hydrolysis catalyst than Cu-zeolite. The observed slip of HNCO at the reactor outlet for the Cu-ZSM-5 catalyst supports previous studies that found HNCO in the exhaust gas downstream the SCR catalyst. [17, 46]

3.2 Spatially Resolved Reaction Kinetics

Spatially resolved concentration profiles are measured in both catalysts during constant dosage of UWS in order to investigate gas and surface reaction kinetics. First, due to the measurement technique, it is important to consider the capillary and its effect on the conversion of the species. This is because the capillary reduces the available space in the channel, which is why the residence time increases and the conversion grows [45]. We estimated the difference in conversion following the literature [47]. The analytical model evaluates the concentrations in an empty channel, which is then compared with one example of experimental data (Fig. S6). This deviation reaches its maximum of 53 % at half of the channel depth, which is also reflected in the outliers of the experimental data (Figs. 2–4).

Considering temperature and residence time, a theoretical, stoichiometric amount for an ideal gas of NH_3 and HNCO was calculated to be 130 ppm each, based on the assumption of a complete thermolysis of urea dosed with 0.5 g min^{-1} UWS feed. The concentration of both species is measured by FTIR using the capillary sampling technique at the catalyst front face. The resulting FTIR data shows that only urea thermolysis occurs in front of the catalyst with approximately 150 ppm NH_3 out of the dosed UWS. As this value is higher than the calculated, stoichiometric amount of NH_3 produced by thermolysis, it is assumed that the spray and ammonia distribution is inhomogeneous over the cross section at the catalyst front face. The capillary position is in the lower half of the flow channel. Since UWS

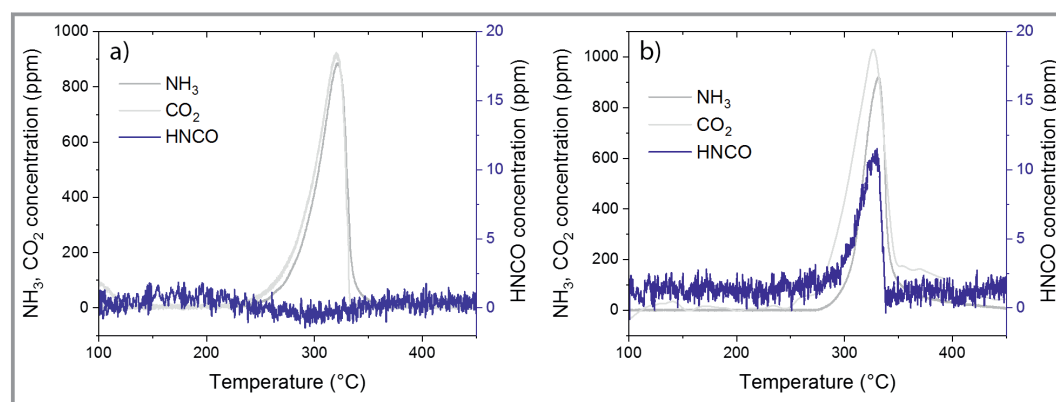


Figure 1. Lab bench test of HNCO hydrolysis over TiO_2 (a) and Cu-ZSM-5 (b). Amount of HNCO and NH_3 measured at the reactor outlet by FTIR. $GHSV = 10\,000 \text{ h}^{-1}$; 500 mL min^{-1} , 5 % H_2O , 10 % O_2 in N_2 .

Table 1. Mass balance of used cyanuric acid compared to resulting products.

	TiO_2 [mg]	Cu-ZSM5 [mg]	TiO_2 [mol]	Cu-ZSM5 [mol]
Initial sample Cyanuric acid	15.06	15.92	$1.2 \cdot 10^{-4}$	$1.2 \cdot 10^{-4}$
Outlet NH_3	5.45	4.75	$2.8 \cdot 10^{-4}$	$2.8 \cdot 10^{-4}$
Outlet HNCO	0	0.19	0	$4.5 \cdot 10^{-6}$
Outlet CO_2	13.02	11.72	$3.1 \cdot 10^{-4}$	$2.8 \cdot 10^{-4}$

is sprayed downwards with an angle of 30° , a higher droplet fraction and ammonia concentration is expected in the lower half of the channel. However, due to an interference of the infrared spectra of HNCO and CO_2 the FTIR overestimates the HNCO concentration slightly. As the thermolysis stoichiometry is 1:1 according to Eq. (1) and since the NH_3 signal remains uncompromised, the amount of HNCO is set to the same value as NH_3 , analogously to a study by Chen et al. (Fig. S4). [43]

Fig. 2 shows results on the spatially resolved species concentration over the vanadia-titania-based catalyst for an experiment with UWS dosing, using ambient air having 1.5% H_2O in the gas feed. Here, both species show a continuous decrease along the length of the catalyst channel. Since oxygen in the air gas stream is the only species that could react with NH_3 , we looked into NO species (Fig. S5). However, only traces are visible, implying another possible way of reaction. Therefore, the majority of NH_3 is assumed to form N_2 and H_2O without any other reactant in the gas phase [48, 49]. Literature shows the potential on zeolite catalysts for 300°C for NH_3 oxidation with similar traces of NO and the formation of N_2 [49]. Neither FTIR nor MS can detect N_2 , thus we assume the same results as literature. Lastly, it is also possible that the vanadia-titania-based catalyst itself stores the NH_3 , which can be explained by the typically strong adsorption of NH_3 on the surface of vanadia-titania-based catalysts [21, 50, 51]. Since our experiment is conducted at 300°C , a full surface coverage with NH_3 is assumed as result, in literature [51] as well as in our experiment. The decrease in concentration diminishes after half of the catalyst length. Thus, either the catalyst is slowly saturated or the production of NH_3 is decreased. During the dosing of the UWS a liquid film is formed out of non-vaporized UWS. This formed film might also add to the production of NH_3 . After the water is evaporated, the liquid film consists of molten urea and by-products. A recent study also discussed the formation of a film containing mol-

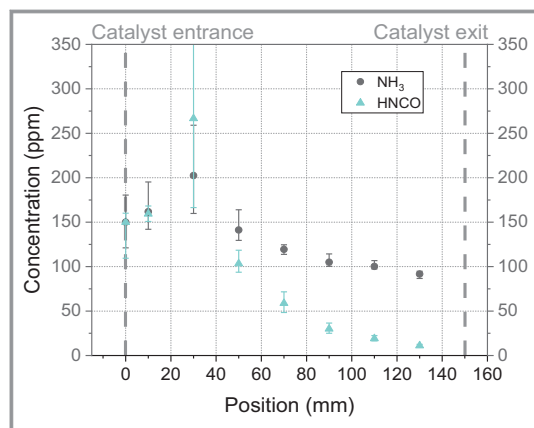


Figure 2. Spatially resolved gas phase concentration profile of HNCO and NH_3 in a monolith coated with a vanadia-titania-based catalyst (600 cps). $T_{\text{Gas phase}} = 300^\circ\text{C}$, $GHSV = 200\,000\text{ h}^{-1}$, 1000 L min^{-1} , 0.5 g min^{-1} UWS, air atmosphere.

ten urea and the by-product biuret [52]. The results of this study, based on in situ laser Raman spectroscopy, show the urea conversion and biuret formation to be affected by H_2O and NH_3 diffusion. Consequently, biuret and urea are potential reaction partners for HNCO before entering the catalyst. This way, only NH_3 enters the catalyst, possibly distorting the HNCO concentration. As a further remark, if HNCO decreases, NH_3 and CO_2 are produced. HNCO is expected to convert rapidly over the catalyst [53]. The decrease of the HNCO concentration along the monolith channel is steeper than for NH_3 , resulting in conversion of over 75% of its initial concentration after half the catalyst length. The remaining 25% convert slower than in the beginning. At the catalyst outlet, approx. 7% of HNCO is still present (approx. 11 ppm). This is in accordance with literature where an HNCO slip of 10 ppm was reported after the catalyst at similar temperatures and initial urea concentrations [46]. End-of pipe FTIR measurements are performed to account for the total gas flow and compare it with the gas flow through the single channel with the capillary. The corresponding results are discussed together with the NO containing gas phase at a later point.

An increase of the NH_3 and HNCO concentration profile can be seen around 30 mm capillary position. Although the measurements were started after the test rig had reached a steady state, fluctuations in concentration of NH_3 and HNCO are observed throughout the dosing period. The setup has small fluctuations in temperature and volumetric flow rate of 0.5–1%. In addition to slight fluctuations in the mass flow during UWS injection, a fluctuation of 15 ppm in the NH_3 and HNCO signal is estimated. Even higher fluctuations are measured in steady-state experiments within a period of 30 min (Fig. S7). These additional higher fluctuations, compared to the estimated ones, are explained by the measuring technique. UWS is dosed by pulsed injection into the channel directly upstream of the catalyst, resulting in local turbulence, varying droplet impact regimes and concentrations. Additionally, the formed liquid film flows downstream, where it begins to evaporate due to the higher wall temperatures, produces HNCO and NH_3 and forms solid by-products, resulting in transient conditions (Fig. S7 and S8). [54] The described transient condition may cause the dosed spray to continuously transport droplets directly to the channel entrance, resulting in thermolysis (cf. Eq. (1)) in the channel itself and therefore an increased concentration at the beginning of the channel.

The addition of steam to the gas phase provides additional OH groups that can facilitate the hydrolysis of HNCO (Eq. (2)). As shown in Fig. 3, an increase in water concentration results in higher conversion of HNCO over the vanadia-titania-based catalyst. Analogous to the results obtained in air only, the first 40–50 mm of the measurement in the presence of water show similar concentration profiles with less pronounced concentration increase due an increased HNCO hydrolysis rate. However, the concentration profiles differ from those obtained under dry conditions,

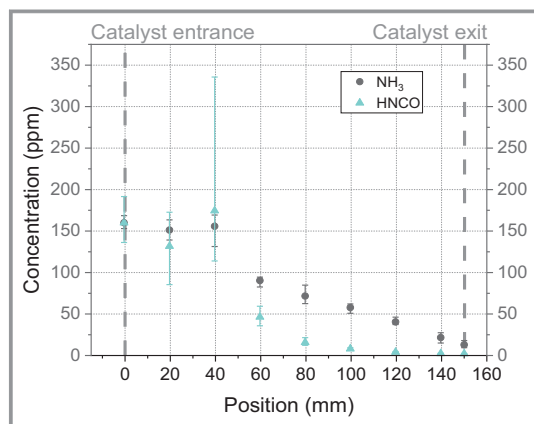


Figure 3. Spatially resolved profile of HNCO and NH₃ within a monolith channel exhibiting a vanadia-titania-based coating (600 cps). $T_{\text{Gas phase}} = 300\text{ }^{\circ}\text{C}$, $GHSV = 200\,000\text{ h}^{-1}$, 1000 L min^{-1} , 0.5 g min^{-1} UWS, 5% H₂O in air atmosphere.

additionally to the now higher measured starting concentration of 160 ppm. In the steam-containing gas atmosphere, the concentration of NH₃ declines almost linearly, whereas HNCO seems to decrease much faster. With only 2% of the initial inlet concentration, the concentration of HNCO at the end of the catalyst channel is less compared to the experiment without steam. Regarding the total conversion the steam improves the hydrolysis, however, a significant length of the SCR catalyst is still used for HNCO hydrolysis.

Fig. 4 shows results of the same experiment but with additional NO dosage. Looking at the error bar, the first few data points are again affected by the fluctuations coming from the UWS dosage and the capillary. The results reveal an earlier decrease for HNCO in the presence of NO (in the first 30 mm) compared to the experiments without NO addition (Fig. 3, at around 60 mm). This behavior is understood by an interaction of NO and HNCO, which uses HONO intermediates to convert HNCO under a different reaction path (Eq. (3)) [55].

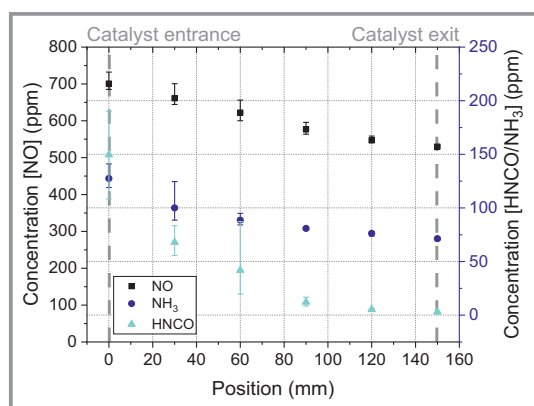
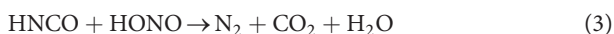


Figure 4. Vanadia-titania-based (600 cps); spatially resolved profile of HNCO, NO and NH₃. $T_{\text{Gas phase}} = 300\text{ }^{\circ}\text{C}$, $GHSV = 200\,000\text{ h}^{-1}$, 1000 L min^{-1} , 0.5 g min^{-1} UWS, 5% H₂O, 700 ppm NO in air atmosphere.



Furthermore, as before, a similar case occurs that about 90% of converted HNCO is reached after two-thirds of the channel. Nevertheless, still over 1% of the initial HNCO concentration remains at the catalyst outlet. In contrary to HNCO, NH₃ is experiencing a slip of 70 ppm. This is equivalent to 50% of the initial concentration.

By comparing the HNCO concentrations measured at the catalyst outlet in all three experiments (Fig. 5), we can conclude that the vanadia-titania-based catalyst efficiently decomposes most of the HNCO, presumably due to the TiO₂ content, which was identified as active species for HNCO conversion [27, 56]. Furthermore, the gas phase composition influences the conversion. Only minor differences are observed, however, the capillary technique reveals the differences in the axial concentration profiles inside the catalytic channel. For the increase in H₂O concentration, the HNCO conversion is promoted in the first half of the catalyst and ensures a fast hydrolysis reaction. The HNCO profile does not significantly change when adding NO to the steam-containing atmosphere. While the reaction between NO and NH₃ predominantly occurs on the V₂O₅ functionality, TiO₂ sites remain mostly unoccupied and therefore active for the hydrolysis of HNCO, hereby ensuring a simultaneous conversion of both species.

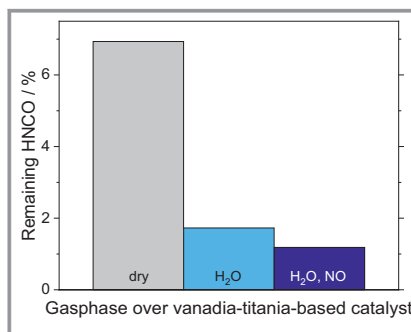


Figure 5. Comparison of the remaining HNCO at the end of the catalyst under different gas atmosphere. $T_{\text{Gas phase}} = 300\text{ }^{\circ}\text{C}$, $GHSV = 200\,000\text{ h}^{-1}$, 1000 L min^{-1} , 0.5 g min^{-1} UWS in air with either 0% H₂O, 5% H₂O, or 5% H₂O and 700 ppm NO.

Since Cu-based catalysts experience growing attention in the field of low-temperature SCR [57, 58], a monolith coated with a Cu-exchanged zeolite washcoat for its activity for HNCO decomposition was investigated, hereby focusing on the more realistic gas atmosphere that contains 700 ppm NO, 5% H₂O and air. The decrease of NO, NH₃ and HNCO is less steep and more stretched out. Furthermore, the urea thermolysis is less pronounced in the beginning of the catalyst compared to the previous results. As shown in Fig. 6, the profile differs from those obtained for the vanadia-titania-based catalyst sample, as the conversion of gaseous species proceeds along the entire length of the catalyst channel. This behavior indicates that the entire catalyst length is needed for both, the deNO_x reaction via SCR with

NH_3 and the HNCO hydrolysis. Compared to the vanadia-titania-based catalyst that had the same length, less NO is converted. With 40 ppm NH_3 and 400 ppm NO at the catalyst exit, we observed a significant undesired slip of both potentially harmful gases, NH_3 and HNCO. These observations are in line with previous studies, which report an NH_3 slip of approx. 10–20 % for Cu-zeolite catalysts operated at 300 °C [59,60]. In addition, the HNCO hydrolysis is slower over the Cu-zeolite catalyst and a small amount of 3 % of the initial HNCO concentration remains at the end of the catalyst (cf. Fig. 6). Note that the Cu-zeolite exhibits 400 cpsi and thus has a bigger channel diameter than the vanadia-titania-based catalyst with 600 cpsi. This results in a smaller velocity but at the same time a smaller flow disturbance in the channel due to the capillary reducing residence time [45]. Thus, for an exact comparison, the same residence time for both catalysts has to be chosen. The vanadia-titania-based catalyst has a total residence time of 0.012 s at the end. This is at 14 cm for the Cu-zeolite. The data in Fig. 7 compares the HNCO concentration of both catalysts. At 14 cm, the concentration for the Cu-zeolite is at 6.7 ppm while the vanadia-titania-based catalyst already has reached 2.5 ppm. Thereby, the shorter residence time in the Cu-zeolite due to the influence of the capillary explains the decreased HNCO conversion by the mass transport limited [25,61,62] hydrolysis compared to the vanadia-titania-based catalyst.

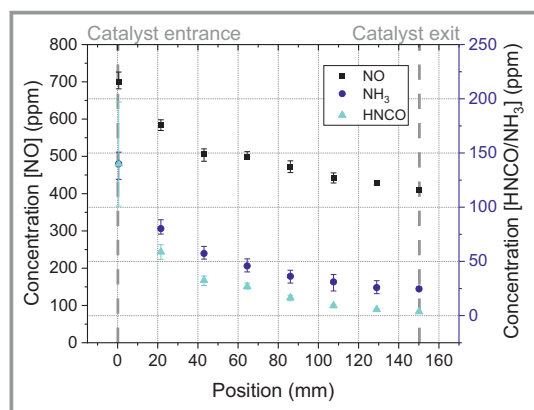


Figure 6. Cu-SCR (400 cpsi); spatially resolved profile of HNCO, NO and NH_3 . $T_{\text{Gas phase}} = 300\text{ }^\circ\text{C}$, $GHSV = 200\,000\text{ h}^{-1}$, 1000 L min^{-1} , 0.5 g min^{-1} UWS, 5 % H_2O , 700 ppm NO in air atmosphere.

When simplifying the result to the active sites, TiO_2 on the vanadia-titania-based catalyst seems to have a clear advantage over the Cu-zeolite. This result is reflected in both Fig. 1 and Fig. 7, demonstrating a faster hydrolysis and higher conversion on TiO_2 . The Cu-zeolite shows less impact on the residence time and less conversion in the powder catalyst experiment but is in a realistic test almost on par with the vanadia-titania-based catalyst, especially when comparing the FTIR results (Fig. S9). Another crucial aspect that needs to be considered when comparing the catalytic activity is the catalyst's aging state. Our results are

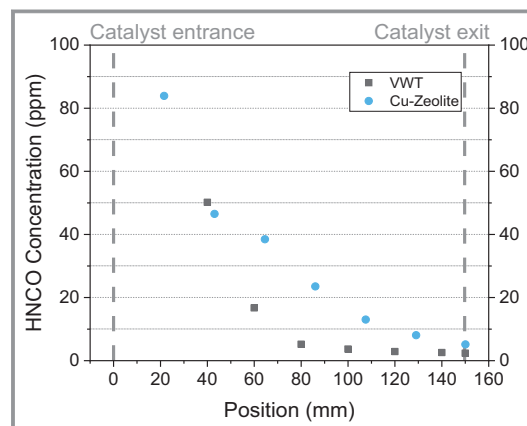


Figure 7. Comparison of HNCO hydrolysis between the vanadia-titania-based catalyst and Cu-zeolite. $T_{\text{Gas phase}} = 300\text{ }^\circ\text{C}$, $GHSV = 200\,000\text{ h}^{-1}$, 1000 L min^{-1} , 0.5 g min^{-1} UWS, 5 % H_2O , 700 ppm NO in air atmosphere.

obtained for a fresh catalyst. After aging and deactivation of the active sites either via V_2O_5 reacting to a less active polymeric species [63], or through the formation of possible barrier layers, activity is assumed to diminish. Already after few experiments, the aging becomes visible at the catalyst front side indicated by the change of colors (Fig. S10). Despite the challenge of aging, HNCO conversion into NH_3 and CO_2 is still possible [16]. However, clear shifts in intensity for CO_2 or NH_3 during the measurement is not observable. This observation can be taken as another indicator for the adsorption of NH_3 on the catalyst.

4 Conclusion

In this study, we investigated the influence of SCR catalysts on the HNCO decomposition via hydrolysis under conditions relevant for lean deNO_x applications. By combining simple decomposition experiments and in situ investigations by means of spatially resolved experiments within two commercial SCR catalyst samples, we evaluated the HNCO hydrolysis activity of a vanadia-titania-based catalyst and a Cu-zeolite catalyst. Spatial profiling revealed that HNCO hydrolysis requires the entire length of the catalyst channel under realistic space velocities. The experiments clearly demonstrate that HNCO is still not fully decomposed at the end of the catalyst, with Cu-zeolite being less efficient compared to the vanadia-titania-based catalyst. Moreover, due to the presence of TiO_2 , the HNCO concentration drop proceeded faster over the vanadia-titania-based catalyst. In the best case of a long residence time of 0.016 s, 2 to 3 % of the initial HNCO concentration are present at the catalyst outlet. Depending on the amount of urea injected the 2 % HNCO left amounts for a HNCO concentration of 10 ppm and above. Additionally, a slow HNCO conversion could result in a possible NH_3 slip. However, if NH_3 is still being generated along the monolith channels, it can only partially participate in the SCR reaction, which decreases the overall

NO_x conversion efficiency. In summary, adjustments on the Cu-zeolite are less likely to achieve an improvement regarding HNCO conversion. Favorable conversion with less catalyst space can be achieved with adaptations in channel size and the content of TiO₂, which are promising approaches for further increasing the efficiency of SCR catalysts for HNCO hydrolysis. Last but not least, the introduction of an additional TiO₂ catalyst for HNCO hydrolysis upstream the SCR catalyst could be a suitable approach for ensuring full HNCO hydrolysis [52, 64].

Supporting Information

Supporting Information for this article can be found under DOI: <https://doi.org/10.1002/cite.202100192>.

The authors kindly acknowledge the financial support from the German Research Foundation (Deutsche Forschungsgemeinschaft, DFG) through project 237267381 – TRR 150. Furthermore, we thank J. Pesek and H. Weickenmeier (ITCP, KIT) for technical support and express our gratitude to Martin Votsmeier (Umicore AG & Co. KG) for fruitful discussions and the provision of commercial SCR catalyst samples. Open access funding enabled and organized by Projekt DEAL.

Abbreviations

cpsi	channels per square inch
GHSV	gas hourly space velocity
FTIR	Fourier-transform infrared
MS	mass spectrometer
SCR	selective catalytic reduction
TGA	thermogravimetric analysis
UWS	urea water solution
VWT	V ₂ O ₅ /WO ₃ -TiO ₂ catalyst

References

- [1] M. Koebel, M. Elsener, M. Kleemann, *Catal. Today* **2000**, *59* (3–4), 335–345. DOI: [https://doi.org/10.1016/S0920-5861\(00\)00299-6](https://doi.org/10.1016/S0920-5861(00)00299-6)
- [2] C. N. Costa, A. M. Efstathiou, *Appl. Catal., B* **2007**, *72* (3–4), 240–252. DOI: <https://doi.org/10.1016/j.apcatb.2006.11.010>
- [3] Y. Liu, J. Zhao, J.-M. Lee, *ChemCatChem* **2018**, *10* (7), 1499–1511. DOI: <https://doi.org/10.1002/cctc.201701414>
- [4] H.-S. Kim, S. Kasipandi, J. Kim, S.-H. Kang, J.-H. Kim, J.-H. Ryu, J.-W. Bae, *Catalysts* **2020**, *10* (1), 52. DOI: <https://doi.org/10.3390/catal10010052>
- [5] M. Borchers, K. Keller, P. Lott, O. Deutschmann, *Ind. Eng. Chem. Res.* **2021**, *60* (18), 6613–6626. DOI: <https://doi.org/10.1021/acs.iecr.0c05630>
- [6] D. T. Koch, E. Eßer, S. Kureti, A. Sousa, *MTZ Motortech. Z.* **2020**, *81* (6), 32–39. DOI: <https://doi.org/10.1007/s35146-020-0234-8>
- [7] P. Lott, U. Wagner, T. Koch, O. Deutschmann, *Chem. Ing. Tech.* **2022**, *94* (3), 217–229. DOI: <https://doi.org/10.1002/cite.202100155>
- [8] W. Brack, B. Heine, F. Birkhold, M. Kruse, G. Schoch, S. Tischer, O. Deutschmann, *Chem. Eng. Sci.* **2014**, *106*, 1–8. DOI: <https://doi.org/10.1016/j.ces.2013.11.013>
- [9] M. Hatanaka, *Bull. Chem. Soc. Jpn.* **2009**, *82* (9), 1149–1151. DOI: <https://doi.org/10.1246/bcsj.82.1149>
- [10] W. Brack, B. Heine, F. Birkhold, M. Kruse, O. Deutschmann, *Emiss. Control Sci. Technol.* **2016**, *2* (3), 115–123. DOI: <https://doi.org/10.1007/s40825-016-0042-2>
- [11] K. W. Ku, J. G. Hong, C. W. Park, K. Y. Chung, S. H. Sohn, *Energy Fuels* **2014**, *28* (9), 5959–5967. DOI: <https://doi.org/10.1021/ef501358j>
- [12] M. D. Leslie, M. Ridoli, J. G. Murphy, N. Borduas-Dedekind, *Environ. Sci.: Processes impacts* **2019**, *21* (5), 793–808. DOI: <https://doi.org/10.1039/c9em00003h>
- [13] M. Koebel, E. O. Strutz, *Ind. Eng. Chem. Res.* **2003**, *42* (10), 2093–2100. DOI: <https://doi.org/10.1021/ie020950o>
- [14] S. D. Yim, S. J. Kim, J. H. Baik, I. Nam, Y. S. Mok, J.-H. Lee, B. K. Cho, S. H. Oh, *Ind. Eng. Chem. Res.* **2004**, *43* (16), 4856–4863. DOI: <https://doi.org/10.1021/ie034052j>
- [15] M. Goldbach, A. Roppertz, P. Langenfeld, M. Wackerhagen, S. Föger, S. Kureti, *Chem. Eng. Technol.* **2017**, *40* (11), 2035–2043. DOI: <https://doi.org/10.1002/ceat.201700261>
- [16] O. Kröcher, M. Elsener, *Appl. Catal., B* **2008**, *77* (3–4), 215–227. DOI: <https://doi.org/10.1016/j.apcatb.2007.04.021>
- [17] R. Suarez-Bertoa, C. Astorga, *Transp. Res. Part D: Transp. Environ.* **2016**, *49*, 259–270. DOI: <https://doi.org/10.1016/j.trd.2016.08.039>
- [18] M. Colombo, I. Nova, E. Tronconi, *Catal. Today* **2010**, *151* (3–4), 223–230. DOI: <https://doi.org/10.1016/j.cattod.2010.01.010>
- [19] A. R. Fahami, T. Günter, D. E. Doronkin, M. Casapu, D. Zengel, T. H. Vuong, M. Simon, F. Breher, A. V. Kucherov, A. Brückner, J.-D. Grunwaldt, *React. Chem. Eng.* **2019**, *4* (6), 1000–1018. DOI: <https://doi.org/10.1039/C8RE00290H>
- [20] A. R. Fahami, I. Nova, E. Tronconi, *Catal. Today* **2017**, *297*, 10–16. DOI: <https://doi.org/10.1016/j.cattod.2017.05.098>
- [21] I. Nova, L. Lietti, E. Tronconi, P. Forzatti, *Catal. Today* **2000**, *60* (1), 73–82. DOI: [https://doi.org/10.1016/S0920-5861\(00\)00319-9](https://doi.org/10.1016/S0920-5861(00)00319-9)
- [22] E. Tronconi, I. Nova, C. Ciardelli, D. Chatterjee, M. Weibel, *J. Catal.* **2007**, *245* (1), 1–10. DOI: <https://doi.org/10.1016/j.jcat.2006.09.012>
- [23] D. Zengel, M. Stehle, O. Deutschmann, M. Casapu, J.-D. Grunwaldt, *Appl. Catal., B* **2021**, *288*, 119991. DOI: <https://doi.org/10.1016/j.apcatb.2021.119991>
- [24] D. Zengel, S. Barth, M. Casapu, J.-D. Grunwaldt, *Catalysts* **2021**, *11* (3), 336. DOI: <https://doi.org/10.3390/catal11030336>
- [25] M. Kleemann, M. Elsener, M. Koebel, A. Wokaun, *Ind. Eng. Chem. Res.* **2000**, *39* (11), 4120–4126. DOI: <https://doi.org/10.1021/ie9906161>
- [26] M. P. Ruggeri, I. Nova, E. Tronconi, J. E. Collier, A. P. E. York, *Top. Catal.* **2016**, *59* (10–12), 875–881. DOI: <https://doi.org/10.1007/s11244-016-0562-6>
- [27] A. Lundström, T. Snelling, P. Morsing, P. Gabrielsson, E. Senar, L. Olsson, *Appl. Catal., B* **2011**, *106* (3–4), 273–279. DOI: <https://doi.org/10.1016/j.apcatb.2011.05.010>
- [28] G. Piazzesi, M. Elsener, O. Kröcher, A. Wokaun, *Appl. Catal., B* **2006**, *65* (3–4), 169–174. DOI: <https://doi.org/10.1016/j.apcatb.2006.01.002>
- [29] Y. Ma, X. Wu, J. Zhang, R. Ran, D. Weng, *Appl. Catal., B* **2018**, *227*, 198–208. DOI: <https://doi.org/10.1016/j.apcatb.2018.01.026>

- [30] A. Grossale, I. Nova, E. Tronconi, D. Chatterjee, M. Weibel, *Top. Catal.* **2009**, *52* (13–20), 1837–1841. DOI: <https://doi.org/10.1007/s11244-009-9354-6>
- [31] M. Börnhorst, C. Kuntz, S. Tischer, O. Deutschmann, *Chem. Eng. Sci.* **2020**, *211*, 115319. DOI: <https://doi.org/10.1016/j.ces.2019.115319>
- [32] D. Schweigert, B. Damson, H. Lüders, M. Börnhorst, O. Deutschmann, *Int. J. Heat Fluid Flow* **2019**, *78*, 108432. DOI: <https://doi.org/10.1016/j.ijheatfluidflow.2019.108432>
- [33] M. Börnhorst, O. Deutschmann, *Prog. Energy Combust. Sci.* **2021**, *87*, 100949. DOI: <https://doi.org/10.1016/j.pecs.2021.100949>
- [34] D. Livio, C. Diehm, A. Donazzi, A. Beretta, O. Deutschmann, *Appl. Catal., A* **2013**, *467*, 530–541. DOI: <https://doi.org/10.1016/j.apcata.2013.07.054>
- [35] T. Schedlbauer, P. Lott, M. Casapu, H. Störmer, O. Deutschmann, J.-D. Grunwaldt, *Top. Catal.* **2019**, *62* (1–4), 198–205. DOI: <https://doi.org/10.1007/s11244-018-1122-z>
- [36] K. A. Karinshak, P. Lott, M. P. Harold, O. Deutschmann, *ChemCatChem* **2020**, *12* (14), 3712–3720. DOI: <https://doi.org/10.1002/cctc.202000603>
- [37] K. Keller, P. Lott, H. Stotz, L. Maier, O. Deutschmann, *Catalysts* **2020**, *10* (8), 922. DOI: <https://doi.org/10.3390/catal10080922>
- [38] F. Maurer, A. Gänzler, P. Lott, B. Betz, M. Votsmeier, S. Loriant, P. Vernoux, V. Murzin, B. Bornmann, R. Frahm, O. Deutschmann, M. Casapu, J.-D. Grunwaldt, *Ind. Eng. Chem. Res.* **2021**, *60* (18), 6662–6675. DOI: <https://doi.org/10.1021/acs.iecr.0c05798>
- [39] R. Horn, N. J. Degenstein, K. A. Williams, L. D. Schmidt, *Catal. Lett.* **2006**, *110* (3–4), 169–178. DOI: <https://doi.org/10.1007/s10562-006-0117-8>
- [40] D. Chan, S. Tischer, J. Heck, C. Diehm, O. Deutschmann, *Appl. Catal., B* **2014**, *156–157*, 153–165. DOI: <https://doi.org/10.1016/j.apcatb.2014.03.009>
- [41] *Spatially Resolved Operando Measurements in Heterogeneous Catalytic Reactors*, Advances in Chemical Engineering (Eds: A. G. Dixon, O. Deutschmann), Academic Press, San Diego, CA **2017**.
- [42] M. Börnhorst, S. Langheck, H. Weickenmeier, C. Dem, R. Suntz, O. Deutschmann, *Chem. Eng. J.* **2019**, *377*, 119855. DOI: <https://doi.org/10.1016/j.ces.2018.09.016>
- [43] Z. Chen, W. Yang, J. Zhou, H. Lv, J. Liu, K. Cen, *J. Zhejiang Univ. Sci. A* **2010**, *11* (11), 849–856. DOI: <https://doi.org/10.1631/jzus.A0900798>
- [44] A. Donazzi, D. Livio, M. Maestri, A. Beretta, G. Groppi, E. Tronconi, P. Forzatti, *Angew. Chem.* **2011**, *123* (17), 4029–4032. DOI: <https://doi.org/10.1002/ange.201007346>
- [45] M. Hettel, C. Diehm, B. Torkashvand, O. Deutschmann, *Catal. Today* **2013**, *216*, 2–10. DOI: <https://doi.org/10.1016/j.cattod.2013.05.005>
- [46] O. Kröcher, M. Elsener, M. Koebel, *Anal. Chim. Acta* **2005**, *537* (1–2), 393–400. DOI: <https://doi.org/10.1016/j.aca.2004.12.082>
- [47] H. Gossler, B. L. Kee, H. Zhu, M. Hettel, O. Deutschmann, R. J. Kee, *Chem. Eng. Sci.* **2016**, *149*, 296–305. DOI: <https://doi.org/10.1016/j.ces.2016.04.033>
- [48] M. Iwasaki, in *Urea-SCR Technology for deNOx After Treatment of Diesel Exhausts*, Fundamental and Applied Catalysis (Eds: I. Nova, E. Tronconi), Springer, New York **2014**.
- [49] T. Yu, J. Wang, Y. Huang, M. Shen, W. Li, J. Wang, *ChemCatChem* **2014**, *6* (7), 2074–2083. DOI: <https://doi.org/10.1002/cctc.201402048>
- [50] H. Liu, C. You, H. Wang, *Chem. Eng. J.* **2020**, *382*, 122756. DOI: <https://doi.org/10.1016/j.ces.2019.122756>
- [51] I. Nova, C. Ciardelli, E. Tronconi, D. Chatterjee, B. Bandl-Konrad, *AIChE J.* **2006**, *52* (9), 3222–3233. DOI: <https://doi.org/10.1002/aic.10939>
- [52] P. Langenfeld, C. Hahn, A. Roppertz, S. Kureti, *Emiss. Control Sci. Technol.* **2019**, *5* (4), 317–327. DOI: <https://doi.org/10.1007/s40825-019-00131-4>
- [53] I. Czekaj, O. Kröcher, *Top. Catal.* **2009**, *52* (13–20), 1740–1745. DOI: <https://doi.org/10.1007/s11244-009-9344-8>
- [54] M. Börnhorst, O. Deutschmann, *Int. J. Heat Fluid Flow* **2018**, *69*, 55–61. DOI: <https://doi.org/10.1016/j.ijheatfluidflow.2017.10.007>
- [55] M. Seneque, F. Can, D. Duprez, X. Courtois, *ACS Catal.* **2016**, *6* (7), 4064–4067. DOI: <https://doi.org/10.1021/acscatal.6b00785>
- [56] G. Piazzesi, O. Kröcher, M. Elsener, A. Wokaun, *Appl. Catal., B* **2006**, *65* (1–2), 55–61. DOI: <https://doi.org/10.1016/j.apcatb.2005.12.018>
- [57] S. Mohan, P. Dinesha, S. Kumar, *Chem. Eng. J.* **2020**, *384*, 123253. DOI: <https://doi.org/10.1016/j.ces.2019.123253>
- [58] J. Du, Y. Shan, Y. Sun, M. Gao, Z. Liu, X. Shi, Y. Yu, H. He, *Appl. Catal., B* **2021**, *294*, 120237. DOI: <https://doi.org/10.1016/j.apcatb.2021.120237>
- [59] D. Chatterjee, T. Burkhardt, M. Weibel, I. Nova, A. Grossale, E. Tronconi, in *SAE World Congress & Exhibition*, SAE International **2007**.
- [60] A. Pant, S. J. Schmieg, *Ind. Eng. Chem. Res.* **2011**, *50* (9), 5490–5498. DOI: <https://doi.org/10.1021/ie200060s>
- [61] P. S. Dhillon, M. P. Harold, D. Wang, A. Kumar, S. Y. Joshi, *Chem. Eng. J.* **2019**, *377*, 119734. DOI: <https://doi.org/10.1016/j.ces.2018.08.120>
- [62] P. Hauck, A. Jentys, J. A. Lercher, *Appl. Catal., B* **2007**, *70* (1–4), 91–99. DOI: <https://doi.org/10.1016/j.apcatb.2005.12.025>
- [63] H. Chen, Y. Xia, R. Fang, H. Huang, Y. Gan, C. Liang, J. Zhang, W. Zhang, X. Liu, *Appl. Surf. Sci.* **2018**, *459*, 639–646. DOI: <https://doi.org/10.1016/j.apsusc.2018.08.046>
- [64] F. Birkhold, U. Meingast, P. Wassermann, O. Deutschmann, *SAE Trans.* **2006**, *115*, 252–262. www.jstor.org/stable/44687485